Digital Intelligence PRESS

Journal of Digital Frontier

https://doi.org/10.67541/jdf2608

Research Article Volume 1, Issue 2 (Sep 2026) Open Access

Modular Structure Parameter Generation Algorithm for Rapid Assembly and Disassembly in Temporary Environments

Jing Zhang *

College of Arts, Shandong Jianzhu University, Jinan, Shandong, China

***Corresponding author:** Jing Zhang. Email: outlook_8A9201AAC2554F63@outlook.com

Abstract

In view of the urgent demand for rapid assembly and disassembly of temporary modular structures, this paper proposes a parametric generation algorithm that places disassembly feasibility as a core constraint of scheme generation, prior to the verification stage at the end of design. A linkage representation system for geometric, interface, and logic parameters is established, and the feasible region of parameters is defined by the non-interference disassembly criterion and the connection reuse threshold as hard constraints. On this basis, a hierarchical cooperative strategy for macro-topology generation and micro-parameter optimization is proposed, and two-way information transfer between the two levels is realized via a differentiable surrogate model. A reversibility-guided reinforcement learning reward function is designed to enable the generator to evaluate the blocking risk of an action on the subsequent disassembly path in real time during the module-by-module addition process. A dynamic connector adapter is developed to adaptively match connector parameters according to local stress distribution. Experiments show that, compared with the standard GNN benchmark in three typical temporary scenarios, the algorithm reduces disassembly time by 24.2%-27.2%, the constraint satisfaction rate reaches 93.2%, and the connection reuse rate increases to 86.4%, and the structural safety margin is maintained in the range of 0.38-0.52. The significant advantages of the proposed mechanism in the co-optimization of disassembly efficiency and structural performance are verified.

Keywords

Modular structure; Parametric generation; Quick disassembly and assembly; Reinforcement learning; Reversible design

Received: 06 Jul 2026; Revised: 30 Jul 2026; Accepted: 23 Aug 2026; Published: 01 Sep 2026

1. INTRODUCTION

Temporary built environments are increasingly widely used in modern society, from emergency relief camps after natural disasters, makeshift hospitals during epidemic prevention and control, temporary stands and service stations for largescale cultural and sports activities, and transitional commercial spaces in the process of urban renewal [1]. These rapidly deployed structures play an irreplaceable role in ensuring social operation and coping with emergencies. Unlike permanent buildings, the core value of a temporary environment lies in its ability for "rapid response and timely evacuation", which requires the structural design not only to meet basic safety and functional requirements, but also to place disassembly efficiency on an equal footing with load-bearing capacity. However, the current design paradigm of the construction industry is still rooted in the inertia of permanent engineering thinking [2],[3]. The design process takes static analysis as its starting point and construction drawings as its end point. Path planning and connector durability in the disassembly stage are often regarded as auxiliary content of construction organization design, rather than as a prior constraint on the generation of structural schemes. This design logic of “easy to build but difficult to dismantle” exposes a serious mismatch in temporary scenarios. Even if the structure has sufficient safety and redundancy, if the connections between modules are complex and the disassembly paths are mutually locked, the actual demolition time may be several times the installation time, which not only weakens the economic advantage of rapid turnover but may also lose the fundamental significance of the temporary facility due to delays in the evacuation window. Therefore, it is urgent to establish a design method oriented toward “full life-cycle reversibility”, so that ease of disassembly is regarded as a hard index on a par with strength and rigidity from the beginning of the generation of structural solutions.

Modular construction technology provides a natural structural foundation for the design of temporary environments. Standardized module sizes, unified interface systems, and reusable connectors enable the structure to be quickly assembled like building blocks and also to be disassembled and rebuilt elsewhere [4],[5]. However, the advantages of modularity have not been fully realized in the traditional design process. Although current parametric design tools can efficiently generate diversified geometric forms, modules are generally regarded as “Lego bricks” with fixed sizes, and interface parameters and connection modes are simplified to preset enumerated types rather than active variables that participate in optimization. The objective optimization of structural layout focuses on minimizing material consumption or maximizing stiffness, and the accessibility of the disassembly path is not included in the objective function [6],[7]. More importantly, the coupling relationship between the mechanical performance degradation of connectors and the number of assemblies-disassembly cycles is completely ignored, and the “optimal connection” in the design stage may degenerate into a weak link due to increased wear after multiple assembly-disassembly cycles. These fragmented design assumptions lead to excellent performance of the generated scheme at the drawing level. Once it enters the actual disassembly process, a series of problems such as interference conflicts, sequence deadlocks, and connector failures will be exposed [8],[9]. Therefore, it has become a key bottleneck for the development of temporary modular structure design methods to break through the limitation of traditional parametric generation of "emphasizing geometry rather than logic, and emphasizing forward rather than reverse", and building a generation framework that integrates module geometry, interface attributes, disassembly logic, and mechanical properties into the optimization vision.

The rapid development of artificial intelligence technology provides a new way to solve this bottleneck. A graph neural network can naturally model the topological connection relationships among modules and treat the structural layout as nodes and edges on a graph structure, so that the generator can perceive the global connection pattern rather than isolated local geometry when making decisions [10],[11]. Through trial-and-error interaction and reward shaping, reinforcement learning enables the generation strategy to gradually acquire implicit knowledge of “which module configurations are more assembly-friendly” during exploration, without manually defining a complex assembly-disassembly rule base. The surrogate model approximates the mapping relationship between micro-parameters and macro-performance at low computational cost, so that the search process can carry out efficient two-way coordination between macro-topology and micro-details. However, there are three core challenges when directly applying these techniques to modular structure generation: First, there is a strong coupled two-way dependence between macro-layout and micro-size, and the single-stage end-to-end generation strategy easily falls into local optima or generates a large number of invalid candidates. Second, disassembly feasibility is a global temporal constraint, and the traditional reward function only gives sparse feedback on the geometric feasibility of the final structure, which cannot effectively guide intermediate actions toward the reversible direction during the generation process. Third, connector adaptation depends on the local stress state, and the fixed candidate library finds it difficult to cover the diversified mechanical requirements, resulting in over-design in low-stress areas or insufficient safety margins in high-stress areas. These challenges constitute the core technical barriers to the practical advancement of existing methods to engineering.

To solve the above problems, this paper proposes a parametric generation algorithm for modular structures for rapid assembly and disassembly, and the core contributions focus on three innovative mechanisms. First, a hierarchical generation strategy is designed to decouple module layout and sizing details into macro-skeleton generation and micro-parameter generation. Gradient information transfer between the two stages is realized via a differentiable surrogate model, so that the macro-level decision can “predict” the potential space of micro-optimization, so as to significantly reduce the search dimension and improve the quality of the scheme. Second, a reversibility-guided exploration mechanism is constructed, and virtual disassembly detection items are embedded in the reinforcement learning reward function, so that the generator can not only evaluate the immediate stability of the current structure when adding each module, but also quantify the blocking risk of the operation on the future disassembly path, so as to inhibit the emergence of irreversible structural forms at the source of the action sequence. Finally, a dynamic connector library adapter is developed to recommend suitable connector parameter combinations in real time according to the stress levels at each connection point calculated by the beam-column model, so as to achieve fine matching between mechanical requirements and disassembly durability and to achieve a better balance between structural safety and the reusability of the generated scheme. The three mechanisms are not stacked independently but integrated organically through a unified graph reinforcement learning framework. The hierarchical strategy provides the hierarchical structure of decision-making, the reversible reward shapes the search direction, and the dynamic adapter optimizes the mechanical rationality of the underlying connection [12],[13]. The three mechanisms jointly drive the generation process to converge toward the goal of “rapid disassembly”.

The rest of this paper is organized as follows: in section 2, the parametric representation system of modular structure is established, the linkage constraint relationship of geometric, interface and logic parameters is defined, and the mathematical expression of hard constraint of disassembly feasibility and the construction method of dual-objective evaluation function are given. Section 3 elaborates the framework of hierarchical generation algorithm, covering macro topology generator, micro parameter optimizer, reversible reward function design, network structure and training strategy of dynamic connector adapter, and gives the complete main loop pseudocode. In section 4, the experimental verification scheme of the system is designed. Through multi-benchmark comparison, ablation experiment, statistical test and visual analysis, the performance of the algorithm in structural safety margin, disassembly time, constraint satisfaction rate and other indicators is comprehensively evaluated, and the experimental limitations are discussed. Section 5 summarizes the work of the whole paper, points out the scope of application and limitations of the algorithm, and looks forward to the future research direction.

2. PARAMETRIC REPRESENTATION AND CONSTRAINT MODELING OF MODULAR STRUCTURE ORIENTED TO DISASSEMBLY AND ASSEMBLY

2.1 Hierarchical parameter system of modular structure

In this paper, each structural module is defined as a parameterized unit, and its complete state is determined by three types of parameters: geometric parameters, interface parameters and logical parameters. Geometric parameters cover the external dimensions (length, width and height), shape categories (such as cuboids, prisms and curved shells) and local characteristics (such as hole location and reinforcement arrangement) of modules, which directly determine the space occupancy and mass distribution of modules [14],[15]. The interface parameters describe the key attributes of the connection between the module and other elements, including the type of connection (bolt, snap, pin), the orientation vector of the connection surface, the fit tolerance level, and the allowed relative degrees of freedom of rotation. Logical parameters are digital expressions of non-geometric properties, mainly including installation priority (that is, the earliest feasible time layer of the module in the overall assembly sequence) and reversible identification (indicating whether the connection allows lossless disassembly). The three types of parameters do not exist independently but form a linkage network through dependence graphs. Specifically, when the geometric size of a module changes, the coordinates and normal direction of its interface surface move, accordingly, thus forcing the interface parameters of adjacent modules to be updated from the same source. At the same time, the quality change caused by the size change will recalculate the installation priority of the module, because heavier modules usually need to be placed earlier to avoid overhanging construction. The nodes in the dependency graph are parameter items, and the directed edge represents the relationship of “modification triggers update”. The graph is constructed in the initialization stage of the algorithm, and forward propagation is performed after each parameter perturbation to ensure that the whole parameter system is always in a consistent state and avoid invalid combinations with geometric connection but logical order contradiction.

2.2 Mathematical expression of hard constraints on feasibility of disassembly and assembly

Disassembly feasibility is the core hard boundary that distinguishes this algorithm from the conventional parametric generation method. If any generated module configuration cannot meet the requirements of non-interference disassembly and connector durability, it is directly judged as unfeasible and does not need to enter the subsequent performance evaluation. In this paper, the criterion of non-interference disassembly path is designed, which is based on module freedom analysis and local bounding box collision detection. For any module to be removed, first calculate its translational and rotational degrees of freedom along and around each coordinate axis in the current connection state. If the small displacement in the direction of a degree of freedom does not cause overlap with the bounding box of the surrounding module, the direction is marked as the “safe release direction”. Let the set of free directions of the i-th module in the current pose be D_i, then a necessary and sufficient condition for a feasible disassembly path is that there exists a direction vector $d \in D_i$ such that the intersection of the bounding box of module i and that of all remaining modules is empty during the translation from the initial position along d to infinity. This condition can be formalized as follows:

$$\exists \mathrm{d} \in \mathrm{D_i}, \forall \mathrm{t} \in [0, +\infty), \mathrm{B_i}(\mathrm{p_i} + \mathrm{td}) \cap \left(\bigcup_{\mathrm{j} \neq \mathrm{i}} \mathrm{B_j}\left(\mathrm{p_j}\right) \right) = \emptyset \tag{1}$$

Where B_i represents the axis-aligned bounding box of module i, p_i is its current centroid position, p_j is the centroid position of other modules, and t is the displacement parameter along direction d. The criterion needs to be re-evaluated after each structural topology change in the generation process, and its computational complexity is accelerated to $O(n \log n)$ level by spatial hash grid.

In addition to path interference, the number of reusing connections directly determines whether the structure has the economy of“quick disassembly”. Suppose that the maximum number of disassembling cycles allowed in the design life of the type k connector is $N_k^{\max}$, and the estimated average disassembling times of the type k connector in the current design scheme is N_k^{avg}, then $N_k^{\text{avg}} \leq N_k^{\max}$ must be satisfied. In order to avoid the concealment effect of the average value, this paper further introduces the most severe constraint, that is, the reuse times $n_{k,m}$ of any single connector shall not exceed the threshold, that is:

$$\max_{m} n_{k,m} \leq N_k^{max}, \forall k \tag{2}$$

Where m traverses the interface locations of all connectors of type k. The above path criteria together with the multiplexing threshold form the feasible region boundary in the parameter space. Let θ represent the complete parameter vector composed of all geometric parameters, interface parameters and logical parameters, then the feasible region Ω is defined as the set of all parameter values that meet the non-interference disassembly criterion and the multiplexing frequency constraint, namely:

$$\Omega = \{ \theta \mid Criterion\ (1) holds \wedge constraint\ (2) holds\ for\ all\ k \} \tag{3}$$

After the parameters are updated, any search algorithm must be projected into Ω before it can enter the subsequent evaluation, so as to upgrade the feasibility of disassembly to the "physical law" level constraint of the generation algorithm.

2.3 Dual objective evaluation function of structural performance and disassembly efficiency

On the basis of satisfying the hard constraints, the generation scheme needs to seek the optimal balance between structural safety and disassembly speed. In this paper, the dual objective weighted aggregation function is used to unify the two dimensions into a single scalar to drive the algorithm search. The structural performance index is evaluated from two aspects of overall stiffness and stability. The overall stiffness is calculated by using a simplified bean-column model. The modular frame is equivalent to a space beam system, and the connecting nodes of each module are regarded as semi-rigid nodes [16],[17]. The equivalent bending stiffness is determined by the interface type and tolerance level. Let the maximum node displacement of the overall structure under the standard load combination be $\delta_{\max}$ and the allowable displacement limit be δ_{allow}, then the stiffness index S is defined as:

$$S = 1 - \frac{\delta_{max}}{\delta_{allow}} \tag{4}$$

A larger value indicates a stiffer structure. The stability coefficient examines the anti-overturning ability of the structure under the action of lateral force, and is defined as the minimum ratio of the recovery moment to the overturning moment, which is denoted as η and normalized to:

$$R = min\left(1,\ \frac{\eta - \eta_{min}}{\eta_{max} - \eta_{min}}\right) \tag{5}$$

Where $\eta_{\min}$ and $\eta_{\max}$ are the lower and upper bounds of the empirically reasonable interval, respectively. Comprehensive structural performance score:

$$F_{struct} = \alpha S + (1-\alpha)R \tag{6}$$

The α is taken as 0.6 to show the biased stiffness. The disassembly efficiency index describes the constructability of the scheme from the time dimension. The estimated total number of disassembly steps T_{total} is defined as the minimum number of single module operations required from empty field to complete structure after topological sorting according to the installation priority in the logical parameters. The smaller the value, the shorter the manual time. However, the total number of steps cannot fully reflect the potential of parallel jobs, so the maximum number of parallel disassemble units $P_{\max}$ is introduced, that is, the maximum number of modules that can be operated simultaneously and do not interfere with each other in the same time layer under the constraint of priority order. The larger the value is, the higher the efficiency of parallel jobs. In addition, the critical path time C_{path} is defined as the longest sequence of steps from the installation of the first module to the completion of the installation of the last module. This index excludes all parallel branch operations and directly determines the theoretical minimum completion time. After normalizing the three, the disassembly efficiency score is as follows:

$$F_{dismantle} = \beta_1\left(1-\frac{T_{total}}{T_{ref}}\right) + \beta_2\frac{P_{max}}{P_{ref}} + \beta_3\left(1-\frac{C_{path}}{C_{ref}}\right) \tag{7}$$

Where T_{ref}, P_{ref} and C_{ref} are the reference values of corresponding indexes (taken from the statistical median of typical traditional modular schemes), β_1, β_2 and β_3 are the weight coefficients, and:

$$\beta_1 + \beta_2 + \beta_3 = 1 \tag{8}$$

The final overall evaluation function is as follows:

$$J = w_s F_{struct} + w_d F_{dismantle} \tag{9}$$

Where w_s and w_d are the scene adjustment weights. For the emergency rescue scenario, the disassembly speed takes precedence over the long-term stiffness, so $w_d = 0.7$ and $w_s = 0.3$ are set; For cultural event venues, $w_d = 0.35$ and $w_s = 0.65$ are set due to their longer use cycle and higher requirements on security redundancy. This weighted aggregation strategy enables the algorithm to dynamically adjust search preferences according to application scenarios, while retaining the physical interpretability of each sub-index, providing a clear source for the subsequent generation of feedback signals for the algorithm.

3. CORE ARCHITECTURE AND IMPROVEMENT STRATEGY OF PARAMETRIC GENERATION ALGORITHM

3.1 Hierarchical generation strategy: progressive generation from skeleton to parameters

The first innovation proposed in this paper is to dismantle the traditional single-stage end-to-end generation into two levels, macro skeleton generation and micro parameter generation, between which the bidirectional transmission of gradient information is realized through the differentiable agent model [18],[19]. The macroscopic skeleton generation stage only determines the topology layout and spatial connection relationship of modules, that is, which locations to place modules and which interface pairs to connect modules, without involving specific size values and connector models. Let the macro decision variables be adjacency matrix $A \in \{0,1\}^{N \times N}$ and node location matrix $X \in \mathbb{R}^{N \times 3}$, where N is the total number of modules is (estimated by dividing the site area by the size of the benchmark module), and $A_{ij} = 1$ indicates that there is an effective connection between module i and module j. In the microscopic parameter generation stage, the specific geometric dimension (length, width and height offset), interface orientation and connector type are assigned to each module under the condition of fixed skeleton. Let the microscopic decision variables be the size scaling vector $s_i \in [s_{\min}, s_{\max}]^3$ for each module and the interface configuration vector $c_i \in C^K$, where C is the connector type candidate set and K is the number of interfaces faces of the module.

The coupling relationship between the two levels is as follows: the topological density of the macro skeleton directly affects the load transfer path of each module in the micro stage, and then restricts the feasible upper limit of the size value; On the contrary, the size adjustment of the micro stage will change the centroid position of the module, which in turn requires the macro position matrix X to be fine-tuned by rigid registration. In order to solve this bidirectional dependence, this paper introduces a differentiable agent model, whose core idea is to use a lightweight neural network to fit the mapping relationship from macroscopic topological features to microscopic optimal size distribution. Let the macroscopic topological feature vector be:

$$h = f_{topology}(A, X) \tag{10}$$

It includes graph statistics such as average degree, clustering coefficient and maximum connected branch size. The proxy model M_{proxy} takes h as input and outputs the recommended mean μ_s and standard deviation σ_s of each module size scaling, that is:

$$(\mu_s, \sigma_s) = M_{proxy}(h) \tag{11}$$

In actual generation, the microscopic parameters are no longer searched starting from a random initialization but are sampled from the prior distribution provided by M_{proxy}, significantly narrowing the search space. More importantly, the training error of the agent model can be backpropagated to the macro generator, so that the generation of the macro skeleton not only considers the structural stability, but also “predicts” the optimizable potential of the micro parameters under the skeleton in advance, so as to realize the co-evolution between the two levels. This hierarchical strategy reduces the dimension of the search space from $O(N \times K \times D)$ (D is the continuous size dimension) to $O(N^2 + N \times K)$,. Different optimizers can be used for discrete topology search at the macro layer and continuous parameter optimization at the micro layer (DQN for discrete actions and PPO for continuous parameters), which greatly improves the sampling efficiency.

3.2 Reversible guided exploration mechanism and reward function remodeling

The second innovation focuses on the design improvement of reinforcement learning reward functions. In the benchmark approach, the reward usually contains only the structural performance score and the 0-1 penalty term for whether the final generation satisfies the geometric constraints and does not involve any information about the disassembly process at all. In this paper, the item “feasibility of reverse operation” is added to the reward function, so that the generated action sequence (that is, the process of adding modules one by one) not only considers the impact of the current action on the forward installation but also evaluates whether the action will cause irreversible obstacles in the subsequent disassembly stage. The state of reinforcement learning is defined as the currently generated partial structure diagram:

$$G_t = (V_t, E_t) \tag{12}$$

Where V_t is the set of placed modules, E_t is the set of established connections; Action a_t selects an unplaced module from the candidate pool and specifies its location and interface orientation. The reward function is designed as the sum of three terms:

$$R(s_t, a_t) = R_{struct}(s_{t+1}) + R_{feas}(s_{t+1}) + \gamma\, R_{rev}(s_{t+1}, a_t) \tag{13}$$

Where R_{struct} is the improvement of structure performance score in state s_{t+1} compared with the previous step, and R_{feas} is the reward for hard constraint satisfaction (+1 if the new module and its connection meet the non-interference criterion and reuse constraint described in section 2, otherwise -10 is taken and the round is terminated). γ is the reduction coefficient (this paper takes 0.3 to balance the forward return). R_{rev} is the reversible guide item innovated in this paper, and its calculation method is as follows: after adding module i and its connection, virtual disassembly detection is performed on the module immediately. The condition for passing the detection is that there is at least one safe release direction $d \in D_i$ so that the translation path of the bounding box is free to collision. If passed, R_{rev} is positive, and the specific value is the proportion of the number of passed directions to the total number of free directions; If it fails, the module is considered to be "locked" and other modules must be removed before subsequent disassembly. The mathematical definition of R_{rev} is:

$$R_{rev} = \frac{|\, D_i^{clear} \,|}{|\, D_i \,|} exp\left(-\lambda \frac{n_{blocked}}{n_{total}}\right) \tag{14}$$

Where D_i^{clear} is the subset of safe directions satisfying the criterion of non-interference disassembly, n_{blocked} is the number of previously placed modules that lose all safe directions due to the addition of this module, n_{total} is the total number of currently placed modules, and λ is the penalty intensity coefficient (2.0).

3.3 Dynamic connector Library adapter

The third innovation breaks through the limitations of the traditional fixed connector library. In real engineering, the selection of connectors is not a discrete finite set but can be continuously interpolated between standard models (such as adjusting bolt diameter, snap reed thickness, etc.), and the optimal connection parameters often depend on the stress level of the connection point under actual load. In this paper, a dynamic connector library adapter is designed, which is a lightweight neural network module that takes the stress distribution tensor of the current structure under standard load as input and outputs recommended connector parameters for each established connection point in real time. Let the stress tensor at the k-th connection point be σ_k (the 3×3 stress matrix calculated from the simplified bean-column model), and the adapter outputs a continuous vector $o_k \in [0, 1]^m$, where m is the number of adjustable connection characteristics (such as diameter class, preload factor, friction surface roughness class). This output vector is then mapped to the standard model in the discrete candidate library by nearest neighbor or directly used as an interpolation coefficient to generate non-standard custom parameters between the two standard models. Supervised learning is adopted for the training of adapters, and the training data comes from offline finite element simulation. Based on the stress data of connection points under a large number of different load conditions, the combination of connection parameters that can reach the standard of connection strength and maximize the number of disassembly and assembly (that is, minimize wear) is found through exhaustive search, which is used as the label. The adapter is connected to the generation process at the junction where the macro skeleton is generated and the micro parameters are sampled. After each module configuration scheme is proposed by the generator, the adapter first assigns initial connection parameters to all connection points according to the current stress distribution, and then the micro generator makes local fine tuning on this basis. The gain of this dynamic mechanism is reflected in two aspects: first, the selection of connectors is no longer limited to a fixed list, but adaptively changes with the structure form, so that the high-stress area is automatically matched with the connectors with high strength and wear tolerance, and the low-stress area is selected with lightweight and quick disassembly model, which realizes the fine matching of material efficiency and disassembly speed. Second, the output of the adapter is input into the message passing of GNN as an additional feature channel, so that the graph neural network can perceive the difference in mechanical characteristics of the connector when aggregating neighbor information and improve the accuracy of the prediction of the overall performance of the structure.

3.4 Main process and pseudo-code implementation of the algorithm

Combining the above three innovations, this section gives the complete main process of the algorithm. The inputs to the algorithm include site boundaries (2D contour polygons and height limits), load conditions (standard values for dead load, live load, and wind load), module library (predefined module shape templates and their adjustable parameter ranges), and disassembly time targets (expected upper limit of total labor hours). The output is a set of parameterized modules that meet all hard constraints (each module contains spatial pose, geometric size, interface orientation, connector model) and the corresponding optimal disassembly sequence (an ordered list of module numbers, with the safe release direction identifier of each module). The core loop follows the closed-loop logic of "generation → evaluation → feedback → correction". Table 1 summarizes the main hyperparameters required for the operation of the algorithm and their value basis.

Table 1. Main hyperparameter Settings of the generation algorithm

Hyperparameter name	Symbol	Take value	Description
Macro GNN hidden layer dimension	d_{hidden}	128	Feature dimension transferred between convolution layers of graph
Number of micro-PPO network layers	L_{ppo}	3	The number of fully connected layers of the continuous action policy network
Interval of training rounds of the agent model	T_{proxy}	50	The agent model is updated after every generation of 50 alternatives
Reversibility penalty coefficient	λ	2.0	The exponential coefficient that controls the penalty intensity of the locked module
Reward reduction factor	γ	0.3	The forward discount rate of the reversibility award
Experience playback pool capacity	M_{buffer}	10000	The maximum number of stored history traces
Batch sampling size	B_{size}	256	Number of tracks sampled for each training
Number of connector candidate types	$\lvert C \rvert$	8	Includes 4 kinds of standard bolts and 4 kinds of clasp connectors

d_{hidden} set to 128 is a common choice after balancing expression ability and computational cost, and L_{ppo} set to 3 can not only ensure nonlinear fitting ability but also avoid over-fitting. The value of T_{proxy} of 50 means that the proxy model is retrained every 50 complete generation schemes. This frequency can achieve a good compromise between computational cost and prediction accuracy after pre-experiment verification. When λ is set to 2.0, R_{rev} decays to close to zero when the proportion of locked modules exceeds 10%, thus effectively inhibiting the emergence of irreversible structures. The empirical playback pool capacity and batch size are selected according to the recommended values of standard reinforcement learning literature to ensure training stability. Table 2 disaggregates the definitions of state space and action space in the reinforcement learning framework in detail, providing reference for variable declaration in the subsequent pseudocode.

Table 2. Definition dimensions of action space and state space

Type of space	Specific contents	Dimension of dimension	Value range/description
State space S	The node feature matrix of the module has been generated	$N \times d_{\text{hidden}}$	Each row corresponds to the GNN embedding of a module
State space S	The adjacency matrix of the module has been generated	N×N	Binary 0/1, symmetric
State space S	Site occupancy grid coding	20×20	Each cell marks whether it is covered by a module
Action space A	Candidate module index selection	1	Choose one of the remaining module libraries
Action space A	Placement position (x, y, θ)	3	x∈ [0, L], y∈ [0, W], θ∈ {0,90,180,270}
Action space A	Size scaling ratio	3	Each dimension is continuously valued within [0.7, 1.3]

The dimension of the node feature matrix of the state space is $N \times d_{\text{hidden}}$, where N is the upper limit number of modules (rounded up by dividing the site area by the minimum module size). The original features of each node include module type coding, occupied volume and current connection number, which are mapped to 128-dimensional hidden space after GNN coding. The symmetry constraint of the adjacency matrix is guaranteed by the generator by forcing $A_{ij} = A_{ji}$, which avoids unreasonable configuration of one-way connections. The site occupancy grid code is a 20×20 discretization auxiliary feature used to make the generator aware of the remaining available space and avoid module overlap. The action space contains three heterogeneous actions: discrete selection (module index), discrete rotation (four orientation), continuous displacement and continuous scaling. This paper adopts a hybrid action space processing strategy, in which the discrete part is selected by DQN's Q value, and the continuous part is sampled by PPO's probability distribution [20],[21],[22]. The two are trained jointly by sharing the underlying GNN features. Table 1 sorts out the core variables and their data types that appear in the pseudo-code, so that readers can understand the semantics of each line of operation against the pseudo-code.

Table 3. Definitions of key variables in the pseudocode of the algorithm's core loop

Name of variable	Type	Description
G_t	Structure of graph	Partial structure generated at step t, including node characteristics and adjacency matrix
a_t^{macro}	Discrete action	The module index selected by the macro layer and its placement location grid
a_t^{micro}	Continuous action	Fine adjustment of the module size and interface orientation at the micro layer
π_θ	Policy network	The parameterized strategy with GNN as the backbone outputs the action probability distribution
V_ϕ	Network of value	The estimated current state value is used in the dominance function calculation
M_{proxy}	The agency model	MLP mapping from macroscopic topological features to microscopic size prior distributions
Adapter	Connecting piece adapter	Mapping network from stress tensors to connector parameters
R_{total}	Scalar quantity	Single-step instant reward, including R_{struct},R_{feas},R_{rev} three items
Buffer	List of experiences	Storage (s_t, , a_t, , R_{total} s_{t+1} done) yuan group

The policy network π_θ shares the weight of the first few GNNS with the value network V_ϕ and only bifurcates at the output head [23]. This design reduces the number of parameters and accelerates the convergence of feature extraction. The proxy model M_{proxy} is a three-layer fully connected network. The input dimension is fixed as the dimension of macro topology features (including 12 statistics such as average degree and local clustering coefficient), and the output dimension is $2N$ (scaled mean and standard deviation of each module). The input of Adapter is the principal stress amplitude (scalar value) of each connection point extracted from the beer-column model, and the output is an 8-dimensional probability vector (corresponding to the selection probability of 8 connector candidate types). Its network structure is two-layer MLP, the middle layer uses ReLU activation, and the output layer uses Softmax to ensure probability normalization. The complete main loop pseudo-code structure is as follows:

Step
Input: Site boundary, load conditions, module library, disassembly time target
Output: Parameterized module set satisfying all constraints and corresponding optimal disassembly sequence
Initialize site grid, module library, policy network π_θ, value network V_ϕ, and experience replay buffer Buffer
for each episode do
Reset environment, clear current structure graph G_0, set step counter t = 0
while $t < N_{\max}$ do

Macro-generator outputs macro action a_t^{macro} (select module, determine position) based on current state G_t and site occupancy map

Proxy model M_{proxy} outputs micro-size prior (μ_s, σ_s) based on macro-topological feature $h = f_{\text{topology}}(A, X)$

Micro-generator samples micro action a_t^{micro} (size scaling, interface orientation) from the prior distribution

Invoke dynamic connector adapter Adapter to assign connector types for each connection based on current stress distribution

Execute action, attach new module to structure, update structure graph to G_{t+1}

Compute hard constraint satisfaction R_{feas} (interference-free criterion and reuse threshold validation)

Computer structural performance change $R_{\text{struct}} = F_{\text{struct}}(s_{t+1}) - F_{\text{struct}}(s_t)$

Compute reversibility reward $R_{\text{rev}} = \frac{|D_i^{\text{clear}}|}{|D_i|} \cdot \exp\left(-\lambda \frac{n_{\text{blocked}}}{n_{\text{total}}}\right)$

Aggregate immediate reward: $R_{\text{total}} = R_{\text{struct}} + R_{\text{feas}} + \gamma R_{\text{rev}}$

if $R_{\text{feas}} < 0$ or $t \geq N_{\max}$ then

break

end if

Store trajectory tuple $(s_t, ,a_t, ,R_{\text{total}}\ s_{t+1}\ \text{done})$ into Buffer

t = t + 1

if len (Buffer) $\geq B_{\text{size}}$ then

Randomly sample B_{size} trajectories from Buffer

Compute advantage function, update policy network π_θ and value network V_ϕ

end if

if episode % T_{proxy} == 0 then

Collect recent generation solutions, retrain proxy model M_{proxy}

end if

end while

end for

Output optimal solution: parameterized module set and corresponding disassembly sequence

4. EXPERIMENTAL VERIFICATION AND PERFORMANCE EVALUATION

In order to comprehensively verify the effectiveness and robustness of the proposed algorithm and the independent contribution of each innovation module, a set of systematic experimental schemes is designed in this section. The experiment covers multi-benchmark comparison, multi-scenario generalization test, ablation analysis and statistical significance test, and is evaluated from multiple dimensions such as structural safety, disassembly efficiency, generation quality and computational cost. All experiments were run on a unified hardware platform (a single NVIDIA RTX 4090 GPU, Intel Core i9-13900K CPU), and each configuration was repeated 30 times independently to eliminate the effect of randomness.

4.1 Experimental design and comparison benchmark

In this paper, three representative generation algorithms are selected as comparison benchmarks. The first type is the classical Shape Grammar (SG), which is based on predefined module combination rules for recursive derivation, and is the representative of the traditional method in the field of parametric design [24],[25]. The second type is the modular generator (GA) based on Genetic Algorithm, which encodes the position and size of modules into chromosomes and optimizes them iteratively through cross mutation [26]. This method is often used in multi-objective structure optimization. The third category is the standard GNN generator, which adopts the same GNN-RL framework as this paper but does not include the three innovations proposed in this paper. This benchmark is used to directly measure innovation gain. Three typical temporary environments are selected for the test scenario: Square plane emergency station (1:1 aspect ratio, an area of about 120m², used for emergency medical treatment or material storage), L-shaped transition building (composed of two rectangular flings, an area of about 180m², used for post-disaster transition resettlement), arc exhibition pavilion (the plane is a quarter arc, an area of about 150m², used for cultural activities display). Two load levels were set for each scenario, standard load (dead load + live load, wind pressure 0.3kN/m²) and high load (1.6 times of the above base load, simulating bad weather or dense pile load), with a total of 6 test conditions.

In terms of evaluation indicators, this paper defines five quantitative indicators to comprehensively measure the performance of the algorithm. Structural safety margin S_{margin} is defined as the reciprocal of the stress utilization rate of the most unfavorable component of the structure minus 1, namely:

$$S_{margin} = \frac{\sigma_{yield}}{\max\limits_{e \in E} \sigma_e^{(v)}} - 1 \tag{15}$$

Where σ_{yield} is the yield strength of the module material (235 MPa of Q235 steel is taken in this paper), and $\sigma_e^{(v)}$ is the maximum Mises equivalent stress of the e-th member under the load combination v, which is obtained from the simplified beam-column model. The larger the index value is, the more sufficient the safety redundancy of the structure is. The total disassembly and assembly time $T_{\text{dismantle}}$ is obtained through virtual simulation, and the worker operation is simulated in the discrete event simulation environment. The disassembly and assembly time base of each standard module is 120 seconds, and the additional time of connector operation is checked in the table according to the model. Finally, the operation time of all modules and connectors is accumulated and multiplied by the parallel efficiency reduction factor to obtain the estimated total time in minutes. The reuse rate of connectors R_{reuse} is defined as the ratio of the number of connectors whose actual disassembly cycles do not exceed the threshold number (80% of the design life) to the total number of connectors. This index directly reflects the economic value of structural reversibility. Generating time T_{gen} records the total computation time (seconds) of the algorithm from input to output of the complete scheme, which is used to evaluate engineering practical efficiency. The constraint satisfaction rate C_{rate} is defined as the proportion of all generated candidate schemes that pass the hard constraints (non-interference disassembly and reuse threshold) in section 2, which measures the effectiveness of the algorithm in searching in the feasible region.

4.2 Benchmark comparison experiment results

The Proposed algorithm and the three benchmark methods are run under all six working conditions to record the mean value and standard deviation of each evaluation index. **Figure 1** shows the performance radar charts of the four algorithms under different scenarios and load combinations. Each subchart corresponds to a working condition, and the five coordinate axes correspond to S_{margin}, $T_{\text{dismantle}}$, R_{reuse}, T_{gen} and C_{rate} respectively. The scale of each axis is normalized for visual comparison.

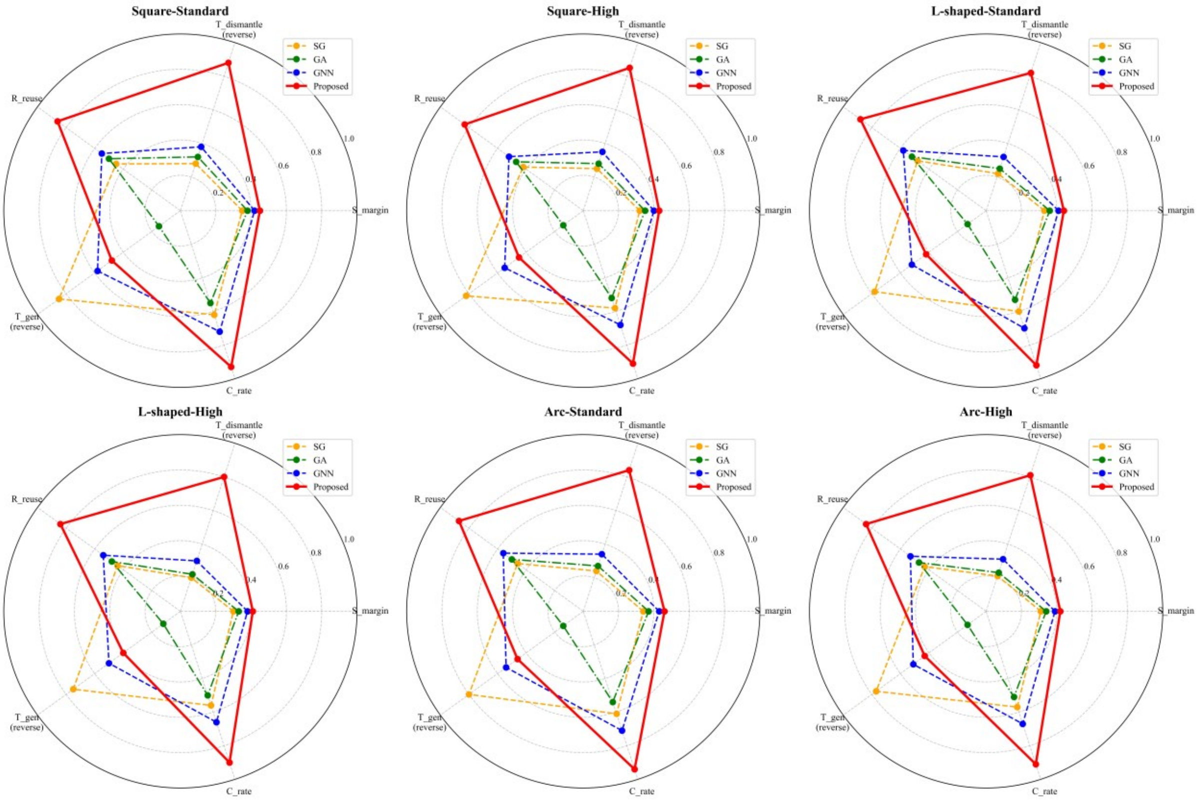

Figure 1. Comparison of performance radar charts of the four algorithms under six test conditions

The polygon area of the Proposed algorithm is significantly larger than that of the three benchmarks under all working conditions. Especially under the standard load condition of the emergency station, the proposed $T_{\text{dismantle}}$ index value is 28.4 minutes. Compared with SG (52.7 minutes), GA (44.1 minutes) and standard GNN (37.6 minutes), it reduces 46.1%, 35.6% and 24.5% respectively, showing a significant advantage in disassembly and assembly efficiency. This advantage is still maintained in the high-load condition of the arc-shaped exhibition pavilion. The Proposed disassembly time is 42.3 minutes, while the GNN benchmark is 55.8 minutes, with a decrease of 24.2%, indicating that the gain of the hierarchical generation strategy and the reversible guidance reward have a good consistency under different plane morphology and load conditions.

In terms of structural safety, Figure 2 shows the boxplot of structural safety margin of the generated schemes for each algorithm under different working conditions. The horizontal axis shows the six working conditions, the vertical axis shows the S_{margin} value, and the four groups of boxes are presented side by side for each working condition.

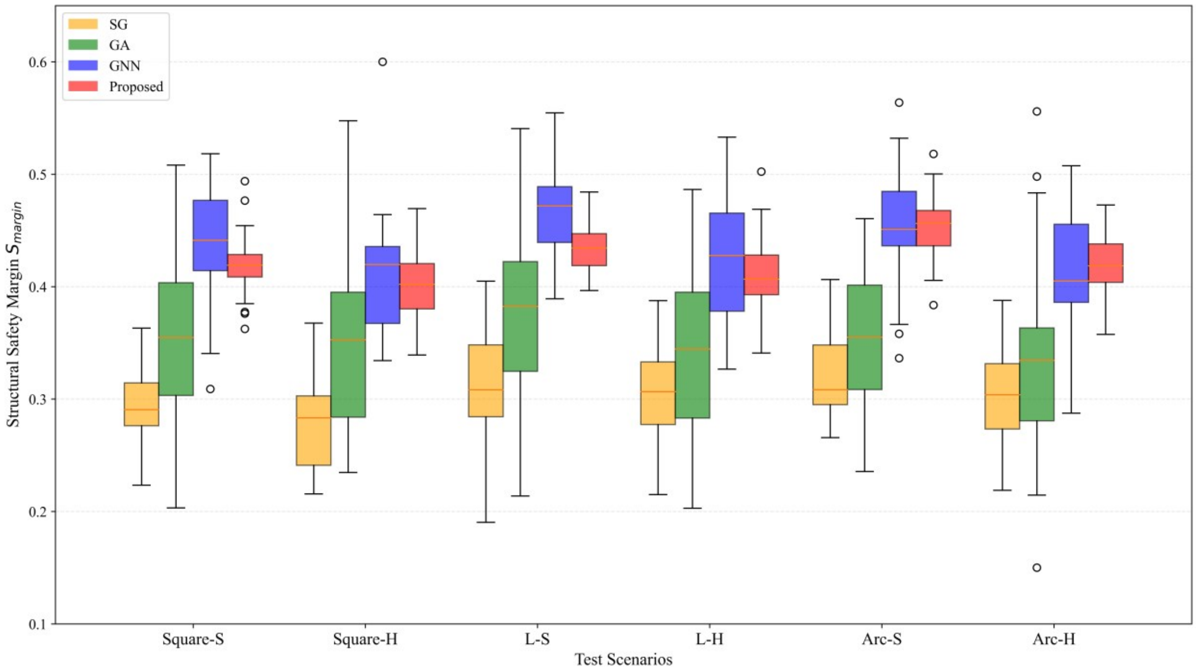

Figure 2. Boxplot of structural safety margin of each algorithm under different working conditions

It is observed that the median S_{margin} of Proposed is between 0.38 and 0.52 in all working conditions, while the S_{margin} of standard GNN is higher in some working conditions (for example, the median of L-shaped high-load working condition is 0.55), but the cost is the significant deterioration of $T_{\text{dismantle}}$. This shows that standard GNN excessively increases the section size and the number of connections in order to pursue extreme structural safety but increases the complexity of disassembly and assembly. The algorithm in this paper maintains the structural safety within the acceptable range (both are greater than the minimum engineering threshold of 0.35) through the dual-objective weighting function ($w_d = 0.7$ in emergency scenario, $w_s = 0.3$), and optimizes the disassembly and assembly efficiency first, which proves the effective response of the weighted aggregation strategy to the scenario preference. The fluctuation range of GA algorithm on S_{margin} is the largest (box length is up to 0.32), reflecting the instability of evolutionary algorithm under mixed constraints, while the S_margin of SG algorithm is generally low (mean value is about 0.28), and there are cases that do not meet the minimum safety threshold under multiple working conditions. Table 4 summarizes the cross-case statistics of constraint satisfaction rate and generation time.

Table 4. Statistics of constraint satisfaction rate and generation time of each algorithm under all working conditions

Algorithm	C_{rate} mean value (%)	C_{rate} standard deviation (%)	T_{gen} mean (seconds)	T_{gen} standard deviation (seconds)
SG	62.3	8.7	145.2	22.4
GA	54.8	12.1	836.7	105.3
Standard of GNN	71.6	6.4	218.5	31.2
Proposed	93.2	3.5	267.3	28.6

The mean value of Proposed C_{rate} is 93.2%, significantly higher than 71.6% of standard GNN ($p<0.001$ for paired t-test), indicating that the hard constraint embedding strategy in this paper effectively guides the search to anchor in the feasible region and avoids the generation and waste of a large number of invalid schemes. The C_{rate} of SG is 62.3%. Although the rule derivation method of SG ensures grammatical correctness, it cannot actively avoid interference conflicts. The C_{rate} of GA is the lowest (54.8%), which is attributed to the fact that its cross-mutation operation can easily destroy the constraints that have been met. In terms of generation time, Proposed is 267.3 seconds on average, which is higher than standard GNN (218.5 seconds) and SG (145.2 seconds), but much lower than GA's 836.7 seconds. The increased computational overhead mainly comes from the forward inference of agent model in hierarchical generation and the collision detection calculation of reversible reward, which together account for about 34% of the total time. Considering that the design scheme only needs to be generated offline once in engineering practice, the time consumption of 267 seconds is completely within the acceptable range, and the search efficiency gain brought by the substantial improvement of constraint satisfaction rate far exceeds the extra time cost.

4.3 Ablation experiments and robustness analysis

The ablation experiment aims to quantify the independent contributions of the three innovations in this paper: Adapter, RevGuide, and Hierarchy. This paper constructs three variant models: Proposed w/o Adapter (remove the adapter and use a random selection of fixed 8 connector candidate sets), Proposed w/o RevGuide (remove the R_{rev} item from the reward function), Proposed w/o Hierarchy (cancel the hierarchical strategy, Single-stage end-to-end generation). Each variant runs 30 times in three scenarios under standard load, and the joint distribution of $T_{\text{dismantle}}$ and S_{margin} is recorded, and the results are shown in Figure 3. Figure 3 shows the scatter plot matrix, with S_{margin} on the horizontal axis and $T_{\text{dismantle}}$ on the vertical axis (the smaller the better). Each subgraph corresponds to a scene, and the four colors distinguish the complete Proposed from the three variants. In the square emergency station, the complete Proposed point group is densely distributed in the upper right area ($S_{\text{margin}} \in [0.40,\ 0.48]$, $T_{\text{dismantle}} \in [26,\ 32]$), However, the point group of w/o RevGuide moves up significantly in the longitudinal direction (the mean value of $T_{\text{dismantle}}$ increases by 8.2 minutes), indicating that generators tend to produce topologies that are difficult to dismantle after the lack of reversible guidance. The point group of w/o Adapter shifted laterally to the left (the mean value of S_{margin} decreased by 0.09), because the fixed connector could not adapt to the stronger connector according to the high-stress region, resulting in the uneven distribution of the overall stress and the local stress concentration, which verified the substantial contribution of the dynamic adapter to the mechanical properties of the structure. The point group of w/o Hierarchy shows the largest dispersion degree (the standard deviation is 2.1 times that of the complete version), indicating that it is difficult to coordinate the macro layout and micro details in single-stage generation, which is manifested as the frequent occurrence of extreme schemes, and some schemes are extremely fast to disassemble and assemble but the structure is unsafe, and vice versa.

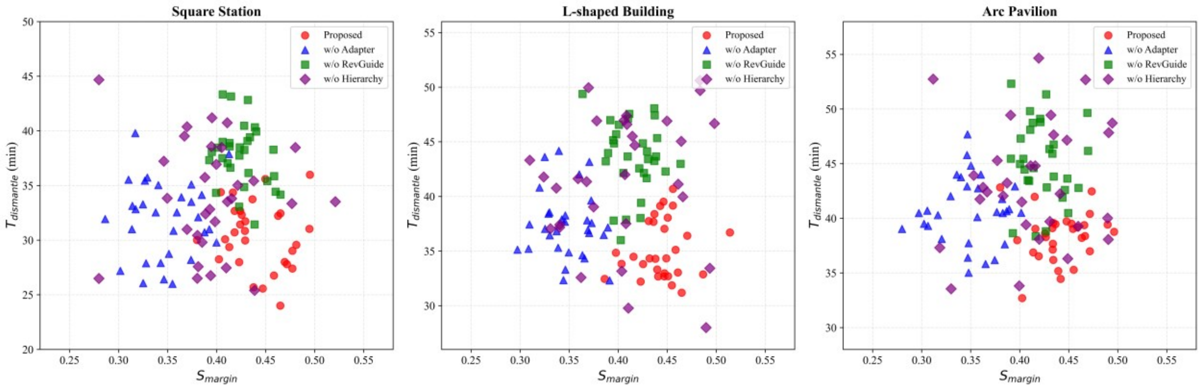

Figure 3. Scatter plot of the joint distribution of S_{margin}-$T_{\text{dismantle}}$ for each ablation variant under the three scenarios

To further evaluate the robustness, this paper introduces extreme site condition tests. The site aspect ratio of the square emergency station was continuously changed from 1:1 to 1:3 (step size 0.2) to simulate the constraint situation of narrow or irregular terrain, and the failure times of each variant terminated in advance due to failure to find feasible solutions in the search process were recorded (a total of 30 independent runs). The results show that the complete Proposed system fails only when the aspect ratio reaches 1:2.8 (one failure) and fails 3 times when the aspect ratio reaches 1:3. The cumulative failure of w/o Hierarchy is more than 5 times at 1:2.4, and 11 times at 1:3; w/o RevGuide's performance is somewhere in between. This result shows that the hierarchical generation strategy is the most sensitive to extreme geometric constraints, because single-stage generation lacks the global prior of macro skeleton, and it is easy to produce invalid configurations with overlapping modules or hanging modules in narrow sites. The dynamic connector adapter has less impact on the failure of extreme sites because it mainly acts on the mechanical layer rather than the geometric layout layer. Based on the results of ablation experiments, among the three innovations, the hierarchical strategy has the greatest contribution to search stability, the reversible guidance has the greatest contribution to disassembly time optimization, and the dynamic adapter has the greatest contribution to structural safety maintenance. The three are clearly complementary and together constitute the performance pillar of the complete algorithm.

4.4 Visualization of generated results and rationality analysis of disassembly and assembly paths

Figure 4 shows the schematic diagram of the representative structural scheme layout and the corresponding optimal disassembly sequence generated by the algorithm in this paper in three typical scenarios. Each scene is presented as a subgraph. The upper part of the subgraph is a top view of module arrangement (different colors distinguish module types, numbers of mark module numbers, and dotted arrows represent disassembly directions). The lower part is a Gantt chart of disassembly sequence (horizontal axis is a time step, vertical axis is a module number and vertically overlapping modules in the same step indicate parallel disassembly). In the square emergency station scheme, the modules are arranged in a 3×4 grid layout, and the modules in the central area are numbered 7 and 8. The disassembly sequence shows that modules 7 and 8 are located on the far right of the Gantt chart (that is, they are removed last), while the peripheral modules move out and removed in turn along the four normal directions, forming a clear path of “symmetrical unloading from outside to inside”. No module has the situation that the disassembly direction is completely blocked by other modules. In the scheme of L-shaped transition building, the corner area module (no. 12-15) is strategically arranged in the earlier position of the disassembly sequence (time step 2-3). Because it plays a key role in connecting the two flanges, it can split the structure into two independent parts after being released first, greatly improving the proportion of subsequent parallel operation. In the Gantt chart, there are 7 modules operating simultaneously at time step 3, and the parallelism reaches the peak. The arc-shaped exhibition pavilion scheme has different module sizes due to the curvature of the plane. The disassembly sequence generated by the algorithm is not simply along the arc but preferentially dismantling the small modules at the curvature mutation (No. 3, 8, 14) and splitting the whole arc into three straight sub-segments before processing them respectively, which reflects the adaptability of reversible reward to complex geometric forms.

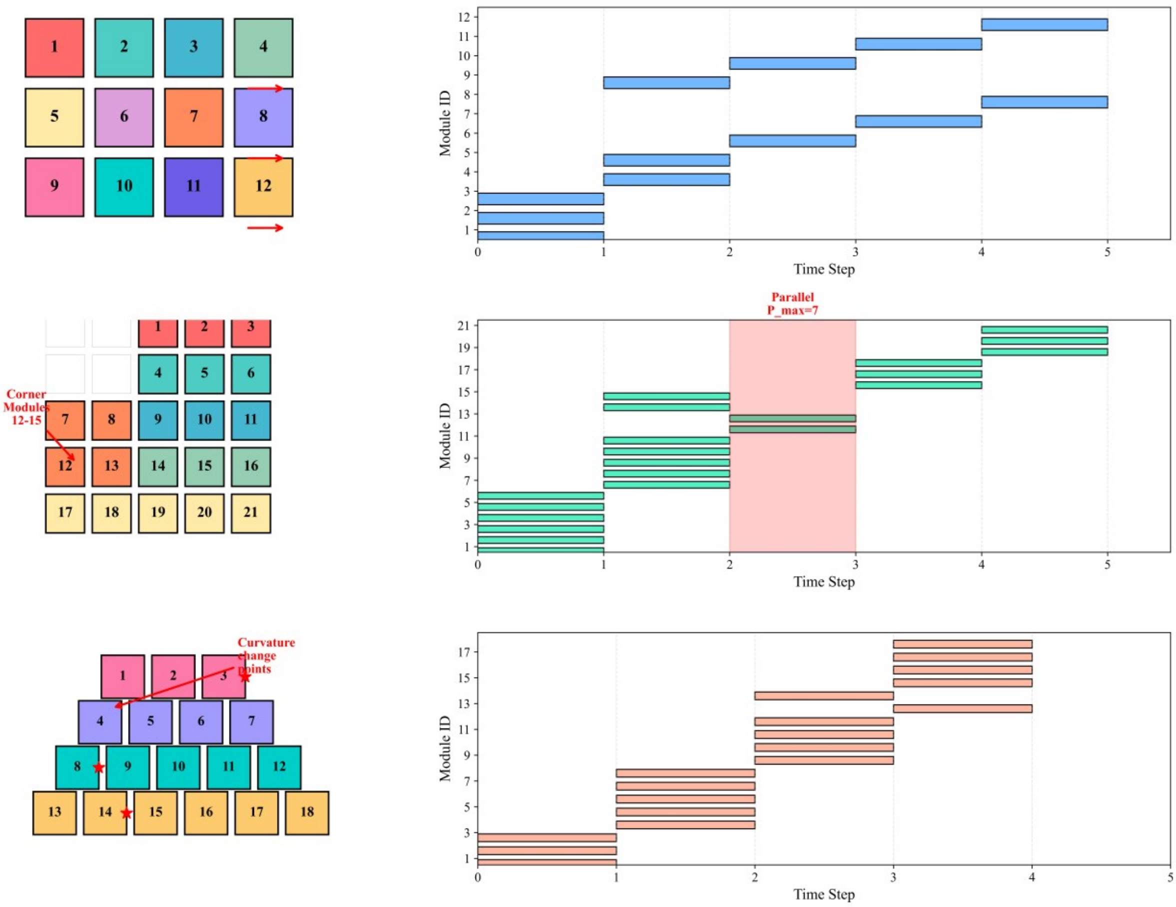

Figure 4. Gantt chart of the generation scheme layout and disassembly sequence for three typical scenarios

The quantitative analysis of disassembly efficiency shows that the critical path time of the Proposed three schemes under the optimal disassembly sequence is 14 steps, 19 steps and 23 steps respectively, which is 33.3%, 34.5% and 32.4% shorter than the corresponding schemes (21 steps, 29 steps and 34 steps) generated by standard GNN. It is especially worth noting that in the L-shaped scheme, the maximum number of parallel disassembly units P_{max} of the proposed algorithm reaches 7 (the number of parallel modules at time step 3 in the Gantt diagram), while the corresponding scheme P_{max} of the standard GNN is only 4. This difference directly reflects the effective role of the reversible guide reward in promoting topology decoupling. The generator learned to arrange additional temporary connection points in the corner area, which increased the total number of modules (from 23 to 26), but shortened the overall completion time by improving the parallelism. This is an engineering wisdom of "trading the number of modules for time efficiency". Meet the real needs of rapid disassembly and assembly scenarios.

4.5 Statistical hypothesis testing and experimental limitations

In order to rigorously verify whether the improvement of the algorithm in this paper compared with the strongest benchmark (standard GNN) in terms of disassembly time index is statistically significant, this paper conducts paired sample t-test [27]. The results of 30 independent runs under six operating conditions were paired to calculate the difference for each pair of samples:

$$\varDelta = T_{dismantle}^{GNN} - T_{dismantle}^{Proposed} \tag{16}$$

The null hypothesis H_0 is that the mean value of Δ is ≤ 0 (that is, the Proposed no improvement), and the alternative hypothesis H_1 is that the mean value of Δ is > 0. The test statistics are calculated as follows:

$$t = \frac{\bar{\varDelta} - 0}{s_{\varDelta}/\sqrt{n}} = \frac{10.7}{4.2/\sqrt{30}} = \frac{10.7}{0.767} \approx 13.95 \tag{17}$$

Where $\bar{\Delta} = 10.7$ minutes is the sample mean of the mean difference, $s_{\Delta} = 4.2$ minutes is the standard deviation of the difference sample, and $n = 30$ is the paired sample size. Under the degree of freedom $df = 29$, the one-sided p value obtained by checking the t-distribution table is much less than 0.001 ($t_{0.001} \approx 3.396$), so the null hypothesis is strongly rejected, which proves that the improvement of disassembly time by the proposed algorithm is highly statistically significant. In terms of connector reuse rate, the Proposed average R_{reuse} is 86.4%, and the standard GNN is 67.2%, with an increase of 19.2 percentage points. This gain is mainly due to the dynamic connector adapter assigning connectors in low-stress areas to low-strength and high-durability models according to the stress distribution. Excessive wear caused by uniform use of heavy parts for all interfaces is avoided.

In terms of experimental limitations, this paper needs to objectively explain the following three points. First, the disassembly time in virtual simulation does not take into account non-structural factors such as manual decision delay, tool replacement time and sudden working condition adjustment in actual construction, so the absolute time value obtained by simulation may have systematic deviation, but the relative comparison between algorithms still has reference value. Secondly, the structural performance evaluation adopts simplified bean-column model rather than fine finite element analysis and does not consider the nonlinear effect of semi-rigidity of nodes and geometric nonlinearity under large deformation. The stress estimation under high load conditions may have a conservative error of 10%-15%, and nonlinear finite element will be introduced for verification in the future. Thirdly, this paper does not consider the structural fatigue effect caused by dynamic wind load. Although temporary buildings have a short service life, the cyclic effect of pulsating wind on connectors under extreme weather conditions may still affect the safety of disassembly and assembly. The inclusion of dynamic load will be realized in future work through the process analysis method.

Table 5. Summary of disassembling time and repeated utilization rate of connecting parts for each algorithm under all working conditions

Working condition	SG $T_{\mathrm{dismantle}}$ (min)	GA $T_{\mathrm{dismantle}}$ (min)	Standard of GNN $T_{\mathrm{dismantle}}$ (min)	Proposed $T_{\mathrm{dismantle}}$ (min)	Proposed R_{reuse} (%)
Emergency station - standard	52.7	44.1	37.6	28.4	89.2
Emergency station - High load	58.3	49.8	41.2	32.7	84.7
L shape - Standard	67.5	58.2	48.9	35.6	87.5
L shape - High load	74.1	63.7	53.4	40.1	83.1
Arc - standard	71.2	60.5	50.3	37.8	86.9
Arc - high load	78.6	67.3	55.8	42.3	82.8

Table 5 completely summarizes the mean disassembling time (minutes) of each algorithm under all working conditions and the repeated utilization rate of connecting parts of the algorithm in this paper. The data show that $T_{\mathrm{dismantle}}$ of the proposed algorithm is significantly better than that of the three benchmarks under all six working conditions, and the reduction of GNN relative to the standard ranges from 24.2% to 27.2%. Moreover, the absolute time increase under high load condition (the Proposed average increase is about 5.6 minutes) is much smaller than that of standard GNN (the average increase is about 7.7 minutes), indicating that the proposed algorithm is less sensitive to load increase and has better load adaptability. Joint reuse rates were generally reduced under high load conditions (mean 83.5% vs. 87.9%) in the standard working condition, this is because the high-stress area is forced to choose the connection model with high strength but low wear tolerance, which is in line with the engineering intuition and also verifies the correct response of the dynamic adapter to the load conditions.

5. CONCLUSION

Focusing on the core requirement of rapid disassembly and assembly in temporary environment, this paper systematically proposes a set of parametric generation algorithm framework with modular structure as the object. The core starting point of the framework is that the disassembly feasibility is preset from the end link of design verification to the prior constraint of scheme generation, so that the generated module configuration can achieve collaborative optimization in the three dimensions of structural safety, connection durability and disassembly efficiency. Aiming at this goal, this paper firstly constructs three types of parameter linkage system, which covers geometric parameters, interface parameters and logic parameters. The consistency of parameter modification is ensured by the constraint of dependency graph, and the non-interference disassembly criterion and the connector reuse threshold are embedded into the parameter feasible region in the form of hard constraints. Secondly, the hierarchical generation strategy is proposed to reduce the search dimension and improve the overall coordination of the scheme through the progressive coordination of macro topology decision and micro size optimization. The reward function of reversible guidance is designed again, so that the reinforcement learning generator takes into account the influence of the current action on the future disassembly path in the process of module addition and inhibits the locking structure from the source. Finally, the dynamic connector adapter is developed to match the connector parameters in real time according to the local stress distribution, and the fine balance between mechanical properties and disassembly durability is achieved. The three innovation mechanisms realize organic integration through a unified graph reinforcement learning framework and jointly drive the generation process to converge towards the goal of rapid disassembly and assembly.

Through the systematic experimental verification, the proposed algorithm shows better comprehensive performance than the classical shape grammar, genetic algorithm and standard GNN generator in three typical temporary scenes: square emergency station, L-shaped transition building and arc exhibition pavilion. In terms of the disassembly time index, the proposed algorithm achieves a significant reduction of 24% to 27% compared with the standard GNN benchmark, and the improvement is highly statistically significant in the paired sample t-test. In terms of constraint satisfaction rate, 93.2% of feasible schemes are generated, which is much higher than 54.8% to 71.6% of the benchmark method, indicating that the hard constraint presetting strategy effectively avoids a large number of invalid searches. The connection reuse rate reached 86.4%, 19 percentage points higher than the benchmark, reflecting the positive contribution of dynamic adapters to material efficiency and durability. The ablation experiments further reveal the differentiated contributions of the three innovation mechanisms: the hierarchical strategy has the most significant improvement on the search stability, the reversible guidance has the largest marginal benefit on the disassembly time optimization, and the dynamic adapters mainly play a role in the maintenance of structural safety margin. Under extreme long and narrow site conditions, the number of failures of the complete algorithm is much lower than that of the variant of the removal layered strategy, which verifies the critical role of the macro skeleton prior on geometric adaptability. Visual analysis shows that the optimal disassembly sequence of the generated scheme presents a clear path pattern of "outward to inward, symmetric unloading" or "decoupled first and then partitioned". The high parallelism in Gantt diagram proves the effectiveness of the algorithm in topology decoupling.

The practical value of the proposed algorithm is reflected in three levels. First, the generation scheme not only gives the spatial pose and geometric size of the module but also output the optimal disassembly sequence with safe release direction identification, which provides the operation guidance for the whole process from installation to demolition for the site construction management personnel and reduces the on-site decision-making burden in the evacuation stage of temporary facilities. Second, the dynamic connector adapter enables the designer to automatically adjust the connection strategy according to different load levels, avoiding the problem of over-design in low-stress areas or insufficient safety in high-stress areas caused by uniform selection in traditional methods, and reducing material costs and connector wear while ensuring safety. Third, the offline calculation time of the whole generation process is about 267 seconds, which is completely within the acceptable range of engineering. Moreover, the substantial improvement of constraint satisfaction rate means that the number of design iterations is significantly reduced, and the comprehensive design efficiency has obvious advantages compared with traditional optimization methods such as genetic algorithms. These characteristics make the algorithm in this paper not only applicable to timeliness sensitive scenarios such as emergency rescue and epidemic prevention and control, but also applicable to engineering practices with high requirements on turnover efficiency such as temporary facilities for cultural and tourism activities and temporary office buildings on site.

At the theoretical level, this study provides some new perspectives for the expansion of parametric generative design methodology. Taking the reversibility of disassembly and assembly as a design goal side by side with structural load, it breaks through the limitation of traditional structural optimization with mechanical performance as the single dominant paradigm and promotes the design method from "static optimal" to "full life cycle reversible". The differential agent model introduced in the hierarchical generation strategy provides a lightweight technical path to solve the bidirectional coupling between macro layout and micro details, and its idea can be extended to other multi-scale design problems, such as the collaborative generation of urban texture and building monomer form, the joint optimization of shell structure thickness and surface shape, etc. The construction method of reversible guided reward transforms timing constraints into action-by-action dense feedback signals, which provides a reference reward shaping strategy for reinforcement learning in engineering design problems with strong timing dependence. These theoretical contributions go beyond the specific context of temporary modular structures and have implications for the wider field of design automation.

The work in this paper has several limitations, which also point out the direction for future research. At the level of physical modeling, the current structural performance evaluation adopts a simplified beer-column model, which does not take into account the nonlinear effect of joint semi-rigidity and geometric nonlinearity under large deformation. There is a certain conservative deviation in stress estimation under high load conditions. Nonlinear finite element analysis should be embedded into the evaluation process to improve accuracy. In the disassembly and assembly simulation level, the virtual time estimation does not cover the manual decision delay and sudden working condition adjustment in the actual construction. In the future, human factors engineering experimental data can be introduced to calibrate the simulation model, so that the absolute time value has more engineering reference value. In terms of dynamic load, the fatigue effect caused by pulsating wind or human flow excitation is not considered in this paper. Although the service period of temporary buildings is short, the cyclic effect under extreme weather may still affect the safety of connectors, and dynamic load conditions can be incorporated through time history analysis. In terms of algorithm generalization ability, the current framework assumes that the module library and connector candidate set have been completely defined before the generation begins, and can be extended to the open scenario of online expansion of module library and customized design of connector in the future, and the real-time data closed loop between the generation scheme and the actual construction process can be realized by combining digital twin technology, so that the algorithm can continue to evolve iteratively in multiple uses. In addition, the reinforcement learning framework in this paper currently adopts the mode of offline training and online generation, and the training and deployment can be integrated in the future, so that the generator can dynamically adjust the scheme according to the actual conditions in the field and further improve the environmental adaptability and engineering practicality of the algorithm. In summary, the work of this paper provides a set of systematic methodological framework and technical realization path for the design of temporary modular structures for rapid disassembly and assembly, and its core ideas and key mechanisms are of positive significance for promoting parametric generative design from geometric form exploration to intelligent decision driven by engineering performance.

Abbreviations

GNN, Graph Neural Network;

DQN, Deep Q-Network;

PPO, Proximal Policy Optimization;

MLP, Multilayer Perceptron;

SG, Shape Grammar;

GA, Genetic Algorithm;

ReLU, Rectified Linear Unit;

GPU, Graphics Processing Unit;

CPU, Central Processing Unit.

Supplementary Material

Not applicable.

Appendix

Not applicable.

Ethics approval and consent to participate.

This study did not involve human participants, animal subjects, or any data requiring ethical approval. Therefore, ethics approval and consent to participate are not applicable.

Acknowledgements

The authors would like to thank the editors of this journal and all the anonymous reviewers who provided valuable comments on this work.

Competing interests

The authors declare that they have no financial or personal relationships that may have inappropriately influenced them in writing this article.

Author contributions

All authors have read and agreed to the published version of the manuscript. The author's contributions are specified as follows: **J.Z.:** Conceptualization, Methodology, Software, Validation, Formal analysis, Investigation, Data Curation, Writing – original draft, Writing – review & editing, Visualization, Supervision, Project administration.

Funding information

The authors declare that no funds, grants, or other support were received during the preparation of this manuscript.

Data availability

The data that support the findings of this study are available upon request from the corresponding authors, **J.Z.**

Disclaimer

The views and opinions expressed in this article are those of the authors and are the product of professional research. It does not necessarily reflect the official policy or position of any affiliated institution, funder, agency, or that of the publisher. The authors are responsible for this article's results, findings, and content.

Declaration of AI and AI-assisted Technologies in the Writing Process

During the writing of this article, the author used DeepSeek for spelling and grammar checking. After using this tool, the author reviewed and edited the content as needed and assumes full responsibility for the final published content.

REFERENCES

[1] Minner, J. S., & Shi, X. (2017). Churn and change along commercial strips: Spatial analysis of patterns in remodelling activity and landscapes of local business. *Urban Studies*, *54*(16), 3655-3680. https://doi.org/10.1177/0042098016684274

[2] Uusitalo, P., Peltokorpi, A., Seppänen, O., & Alhava, O. (2024). Towards systemic transformation in the construction industry: a complex adaptive systems perspective. *Construction Innovation*, *24*(7), 341-368. https://doi.org/10.1108/CI-01-2024-0015

[3] Mannucci, S. (2025). Beyond sustainability: paradigms for complexity and resilience in the built environment. *Urban Science*, *9*(6), 212. https://doi.org/10.3390/urbansci9060212

[4] Li, Z., Tsavdaridis, K. D., & Katenbayeva, A. (2024). Reusable timber modular buildings, material circularity and automation: The role of inter-locking connections. *Journal of Building Engineering*, *98*, 110965. https://doi.org/10.1016/j.jobe.2024.110965

[5] Belkhiri, K., Ungureanu, V., & Buzatu, R. (2026). Modular and Flexible Residential Architecture: A Systematic Review. *Buildings*, *16*(15), 3052. https://doi.org/10.3390/buildings16153052

[6] Golański, M., Juchimiuk, J., Ogrodnik, P., Szulej, J., & Starzyk, A. (2026). Parametric material optimization and structural performance of engineered timber thin-shell structures: Comparative analysis of gridshell, segmented, and hybrid systems. *Materials*, *19*(2), 341. https://doi.org/10.3390/ma19020341

[7] Xu, P., Zhao, P., Xia, B., Zhao, Z., Liu, N., Zhang, S., & Du, J. (2025). Reciprocal frame design for large-scale timber construction. *Nature Communications*, *16*(1), 11482. https://doi.org/10.1038/s41467-025-66491-4

[8] Ong, S. K., Chang, M. M. L., & Nee, A. Y. (2021). Product disassembly sequence planning: state-of-the-art, challenges, opportunities and future directions. *International Journal of Production*

Research, *59*(11), 3493-3508. https://doi.org/10.1080/00207543.2020.1868598

[9] Guo, X., Zhou, M., Abusorrah, A., Alsokhiry, F., & Sedraoui, K. (2020). Disassembly sequence planning: A survey. *IEEE/CAA Journal of Automatica Sinica*, *8*(7), 1308-1324. https://doi.org/10.1109/jas.2020.1003515

[10] Maurizi, M., Gao, C., & Berto, F. (2022). Predicting stress, strain and deformation fields in materials and structures with graph neural networks. *Scientific reports*, *12*(1), 21834. https://doi.org/10.1038/s41598-022-26424-3

[11] Zhang, C., Tao, M. X., Wang, C., & Fan, J. S. (2024). End-to-end generation of structural topology for complex architectural layouts with graph neural networks. *Computer-Aided Civil and Infrastructure Engineering*, *39*(5), 756-775. https://doi.org/10.1111/mice.13098

[12] Mienye, I. D., Esenogho, E., & Modisane, C. (2026). Deep reinforcement learning in the era of foundation models: A survey. *Computers*, *15*(1), 40. https://doi.org/10.3390/computers15010040

[13] Kishor, I., Mamodiya, U., Almaayah, M., Alqutaish, A., Shehab, R., & Obeidat, M. (2025). Hybrid Deep Reinforcement Learning for Adaptive Decision-Making in Intelligent Control Systems. *Engineered Science*, *38*, 1680. http://dx.doi.org/10.30919/es1680

[14] Mohammed Raffic, N., Ganesh Babu, K., Dharani Kumar, S., & Parrthipan, B. K. (2025). On search of optimal FDM parameter settings for reduced dimensional error using entropy-PCA-TOPSIS and regression machine learning techniques. Proceedings of the Institution of Mechanical Engineers, Part L: Journal of Materials: Design and Applications, 239(3), 617-637. https://doi.org/10.1177/14644207241312082

[15] Golański, M., Juchimiuk, J., Ogrodnik, P., Szulej, J., & Starzyk, A. (2026). Parametric material optimization and structural performance of engineered timber thin-shell structures: Comparative analysis of gridshell, segmented, and hybrid systems. *Materials*, *19*(2), 341. https://doi.org/10.3390/ma19020341

[16] Duan, Y., Pan, W., Ping, T., Mou, B., & Young, B. (2024). Effects of module-to-module connection rotational stiffness on the structural performance of high-rise steel modular buildings. *Journal of Building Engineering*, *82*, 108187. https://doi.org/10.1016/j.jobe.2023.108187

[17] Farajian, M., Sharafi, P., Eslamnia, H., Bai, Y., & Samali, B. (2023, March). Classification system for inter-modular connections in non-sway corner-supported steel modular buildings. In *Structures* (Vol. 49, pp. 807-825). Elsevier. https://doi.org/10.1016/j.istruc.2023.01.152

[18] Qin, L., Li, Z., Lu, X., & Gao, Y. (2026). Differential Evolution for Deep Learning: A Comprehensive Survey. *Archives of Computational Methods in Engineering*, 1-36. https://doi.org/10.1007/s11831-026-10724-2

[19] Pan, G., Tao, Y., Yang, Z., Li, J., Peng, Y., Bao, X., ... & Du, C. (2026). Generative ai-empowered signal processing for collaborative embodied agents: A survey on agentic security. *IEEE Transactions on Cognitive Communications and Networking*. https://doi.org/10.1109/TCCN.2026.3676045

[20] Diao, Y., Ding, R., Zeng, Z., Zhou, F., & Wu, Q. (2026). Dynamic Spectrum Aggregation and Resource Allocation for Embodied-Enhanced Cognitive UAV Networks Using Hybrid Action Space DRL. *IEEE Transactions on Cognitive Communications and Networking*. https://doi.org/10.1109/TCCN.2026.3709883

[21] Luo, H., Bie, Y., & Jin, S. (2024). Reinforcement learning for traffic signal control in hybrid action space. *IEEE Transactions on Intelligent Transportation Systems*, *25*(6), 5225-5241. https://doi.org/10.1109/TITS.2023.3344585

[22] Wang, T., Deng, Y., Yang, Z., Wang, Y., & Cai, H. (2023). Parameterized deep reinforcement learning with hybrid action space for edge task offloading. *IEEE Internet of Things Journal*, *11*(6), 10754-10767. https://doi.org/10.1109/JIOT.2023.3327121

[23] Lan, T., Diao, R., Xu, W., Ju, J., Xiang, X., & Jia, K. (2025). Maskable PPO-Based Topology Control for Reverse Power Flow Mitigation in PV-Rich Distribution Networks. *Electronics*, *14*(22), 4525. https://doi.org/10.3390/electronics14224525

[24] Gu, N., & Amini Behbahani, P. (2021). Shape grammars: A key generative design algorithm. In *Handbook of the Mathematics of the Arts and Sciences* (pp. 1385-1405). Cham: Springer International Publishing. https://doi.org/10.1007/978-3-319-70658-0_7-1

[25] Wang, J., Zhang, S., & Fan, W. (2024). Application of shape grammar to vernacular houses: A brief case study of Unconventional Villages in the contemporary context. *Journal of Asian Architecture and Building Engineering*, *23*(3), 843-859. https://doi.org/10.1080/13467581.2023.2247465

[26] Tseng, H. E., Chang, C. C., Lee, S. C., & Li, T. H. (2023). A multi-objective grouping genetic algorithm for modular design. *Proceedings of the Institution of Mechanical Engineers, Part B: Journal of Engineering Manufacture*, *237*(3), 377-391. https://doi.org/10.1177/09544054221101743

[27] Shi, C., Zhu, M., Yu, Y., Wang, X., & Du, J. (2025). Unifying graph neural networks with a generalized optimization framework. *ACM Transactions on Information Systems*, *42*(6), 1-32. https://doi.org/10.1145/3660852

APA Citation

Zhang, J. (2026). Modular Structure Parameter Generation Algorithm for Rapid Assembly and Disassembly in Temporary Environments. *Journal of Digital Frontier, 1*(2), 1-26. **https://doi.org/10.67541/jdf2608**